Supporting Information

Unconventional-Phase Engineering of RuGa Intermetallics Boosting Alkaline Hydrogen-Electrode Reactions

Chang Yang,[a] LuluAn,[a] Zhensheng Mi,[b] Guangzhe Wang,[b] Chenhao Zhang,[a] Weijie Kong,[a] Junhao Yang,[a] Li Xiao,[b] Lin Zhuang[b] and Deli Wang*[a]

a. Key Laboratory of Material Chemistry for Energy Conversion and Storage (Ministry of Education), Hubei Key Laboratory of Material Chemistry and Service Failure, School of Chemistry and Chemical Engineering, Huazhong University of Science and Technology, Wuhan, Hubei, 430074, P. R. China.

b. College of Chemistry and Molecular Sciences, Hubei Key Lab of Electrochemical Power Sources, Wuhan University, Wuhan 430072, China

*Corresponding author
E-mail address: wangdl81125@hust.edu.cn

Experimental Section

Chemicals.

Gallium (III) nitrate hydrate ($GaNO_3 \cdot xH_2O$) and Ruthenium (III) chloride hydrate ($RuCl_3$) were purchased from Shanghai Aladdin Biochemical Technology Co. Ltd. Potassium hydroxide (KOH) were purchased from Sinopharm Chemical Reagent Co. Ltd (Shanghai, China). Ultrapure water with a resistivity of 18.2 MΩ cm was used in all experiments.

Materials Synthesis.

RuGa/C catalysts were prepared via an impregnation reduction method. In detail, $GaNO_3 \cdot xH_2O$ (37.95 mg) and $RuCl_3$ (20.52 mg) were dissolved in deionized (DI) water. 40.0 mg of Vulcan XC-72 was dispersed into the above solution and then sonicated for 30 min. The mixed solution was then transferred to a magnetic agitator to evaporate the water at 65 ^oC, accompanied by sustaining stirring and ultra-sonication. The resulting dark powder was reduced in a tube furnace at 600, 700, and 800 ^oC under a flowing 10 % H_2/Ar atmosphere for 2 h, and the products were named RuGa/C-600, RuGa/C-700, and RuGa/C-800 respectively.

The synthesis of Ru/C was similar to that of the RuGa/C as described above, except for the absence of potassium nitrate and a reduction temperature of 300 ^oC in the tube furnace.

Physical Characterizations

Powder X-ray diffraction (XRD) patterns were collected on the X-ray diffractometer (SmartLab SE, Rigaku) with Cu-Kα radiation (λ=0.1541 nm). TEM images were collected using a Hitachi H-7650 transmission electron microscope with 100 kV acceleration voltage. HRTEM images and EDX mappings were obtained using a probe spherical aberration corrected JEM-ARM200F microscope with 200 kV accelerating voltage. XPS spectra were obtained using an X-ray photoelectron spectrometer (K-alpha, Thermo Scientific) with a monochromatic Al Kα X-ray source (hυ=1486.6 eV). In-situ electrochemical attenuated total reflectance surface-enhanced infrared absorption spectroscopy (ATR-SEIRAS) measurements were performed in a custom glassy cell equipped with a semicylindrical Si prism as an infrared optical window. Ru/Ga molar ratios were determined by inductively coupled plasma optical emission spectrometry (ICP-OES).

LRO Calculation

The long-range ordering degree (LRO) of samples was estimated according to the previous report[1], which is as follows:

$$LRO = \frac{I_{100} / I_{110}}{I_{100}^{*} / I_{110}^{*}} \times 100\%$$

where I_{100} and I_{110} represent the diffraction peak intensities of the superlattice and the fundamental lattice of the sample, respectively; I_{100}^{*} and I_{110}^{*} represent the

corresponding peak intensity to the perfectly ordered structure from the standard card (LRO=100%).

Electrochemical Test

The electrochemical tests were carried out in a standard three-electrode system using a CHI760E electrochemical workstation, in which a graphite rod and a reversible hydrogen electrode (RHE) served as the counter and reference electrode, respectively. The working electrode was a glassy carbon rotating disk electrode (RDE) with a diameter of 5 mm and an area of 0.196 cm^2. For HOR testing, 1 mg of catalyst, 3 mg of Vulcan XC-72, and 1mL of as-prepared Nafion/iso-propanol (0.1 wt% Nafion) solution were mixed and ultrasonically dispersed for 30 min to prepare the homogeneous ink. Then 6 μL ink was loaded on the surface of the RDE and natural drying. For HER testing, 5 mg of catalyst and 1mL of as-prepared Nafion/iso-propanol (0.1 wt% Nafion) solution were mixed and ultrasonically dispersed for 30 min to prepare the homogeneous ink. Then 10 μL ink was loaded on the surface of the RDE and natural drying. All the polarization curves were iR-corrected.

Cyclic voltammetry (CV) curves were conducted in N_2-saturated electrolyte at a scan rate of 50 mV s^{-1}. For the HOR test, the polarization curve was conducted in H_2-saturated 0.1 M KOH by using linear sweep voltammograms (LSV) with a rotation rate of 1,600 rpm and scanning rate of 5 mV s^{-1}. The accelerated durability tests were conducted by potential cycling in the range of 0.05-0.4 V versus RHE for 2,000 cycles with a scan rate of 200 mV s^{-1}. Chronoamperometry (CA) was performed at an overpotential of 50 mV. For the HER test, the polarization curve was conducted in H_2-saturated 1.0 M KOH by using LSV with a rotation rate of 1,600 rpm and scanning rate of 5 mV s^{-1}. The accelerated durability tests were conducted by potential cycling in the range of -0.025-0 V versus RHE for 10,000 cycles with a scan rate of 50 mV s^{-1}. The electrochemical impedance spectroscopy (EIS) measurements were performed at an applied potential -0.03V with the scanning frequency values ranging from 100 kHz to 0.01 Hz. Chrompotentiometry (CP) was performed at a current density of 10 mA cm^{-2}.

The electrochemically active surface area (ECSA) was determined by the CO-stripping voltammetry[2]. The value of ECSA was calculated via equation (1),

$$\mathrm{ECSA} = \frac{\mathrm{Q_{co}}}{(\mathrm{m} \times 420\ \mu\mathrm{C\ cm^{-2}})} \qquad \text{* MERGEFORMAT (1)}$$

where m is the mass loading of noble metal on the electrode.

The electrochemical double layer capacitance (C_{dl}, mF cm^{-2}) of the catalytic surface was obtained according to cyclic voltammetry curves (CV) in the non-Faraday region at various scan rates (20, 40, 60, 80 and 100 mV s^{-1}). The value of C_{dl} was calculated via equation (2),

$$\mathrm{C_{dl}} = \frac{\Delta \mathrm{J}}{\mathrm{v}} \qquad \text{* MERGEFORMAT (2)}$$

where ΔJ means the current density (mA cm^{-2}) difference between the anodic and cathodic sweeps (J_{anodic} - $J_{cathodic}$) at the middle potential versus scan rate (v, mV s^{-1}).

The kinetic current density (j_k) was calculated by the Koutecky-Levich equation (3),

$$\frac{1}{j} = \frac{1}{j_k} + \frac{1}{j_d} = \frac{1}{j_k} + \frac{1}{\beta c_0 \omega^{1/2}} \qquad \text{* MERGEFORMAT (3)}$$

where j, j_d, β, c_0 and ω represent the current density, diffusion-limited current, Levich constant, solubility of H_2 in alkaline solution, and rotation speed, respectively.

The exchange current density (j_0) was calculated by two methods. One is from the Butler-Volmer equation,

$$j_k = j_0\left(e^{\frac{\alpha F}{RT}\eta} - e^{\frac{-(1-\alpha)F}{RT}\eta}\right) \qquad \text{* MERGEFORMAT (4)}$$

Another is to perform linear fitting in micro-polarization regions via the Bulter-Volmer equation,

$$j_0 = \frac{j}{\eta}\frac{RT}{F} \qquad \text{* MERGEFORMAT (5)}$$

where α, F, T, R, and η refer to the charge transfer coefficient, Faraday constant, operating temperature (303 K in this work), the universal gas constant (8.314 J mol^{-1} K^{-1}) and the overpotential, respectively.

The turnover frequency (TOF) of samples was estimated according to the previous report[3], which is as follows:

$$TOF = \frac{\#H_2}{N_{active}^{cat.}} \times 100\%$$

$$\#H_2 = |j| \times 3.12 \times 10^{15}$$

$$N_{active}^{cat.} = \frac{m}{M} \times N_A$$

where $\#H_2$, $N_{active}^{cat.}$, j, m, M, and N_A represent the total number of hydrogen turnovers, number of active sites, current density (mA cm^{-2}), loading of noble metal on the electrode (mg cm^{-2}), molar mass of noble metal (g mol^{-1}), and Avogadro constant (6.022 × 10^{23} mol^{-1}), respectively.

Supplementary Figures

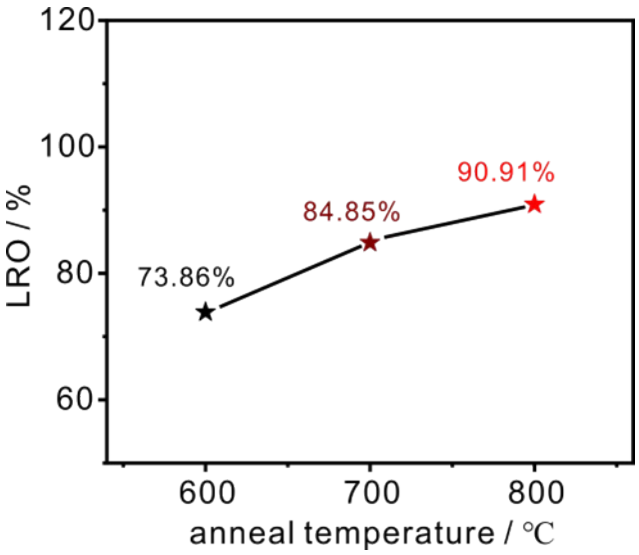

Fig. S1 Long-range ordering (LRO) degrees of RuGa/C-600, RuGa/C-700, and RuGa/C-800.

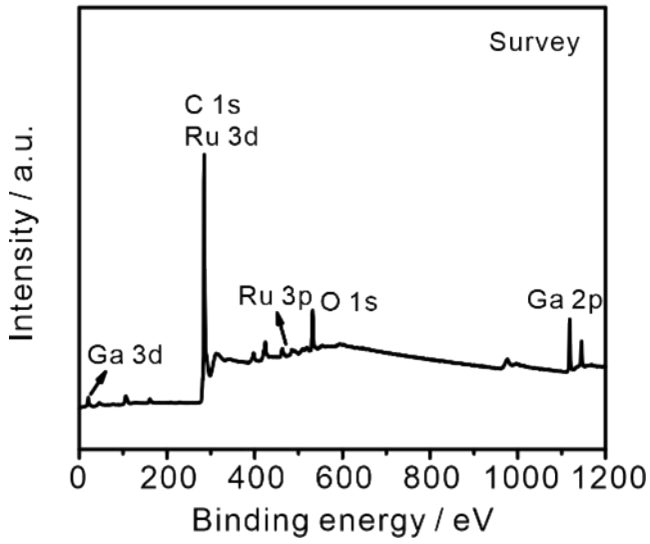

Fig. S2 The XPS spectrum of RuGa/C-600.

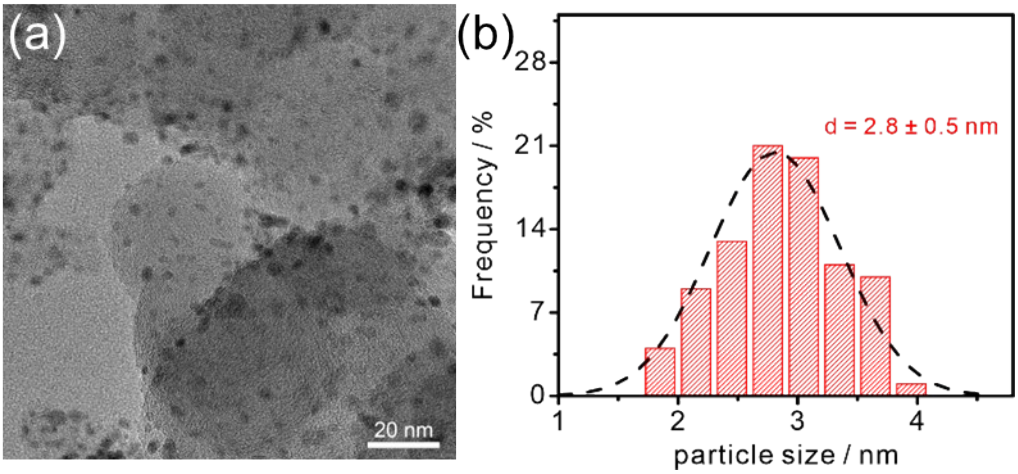

Fig. S3 (a) Low-magnification TEM image of Ru/C and (b) corresponding histogram of particle size distribution.

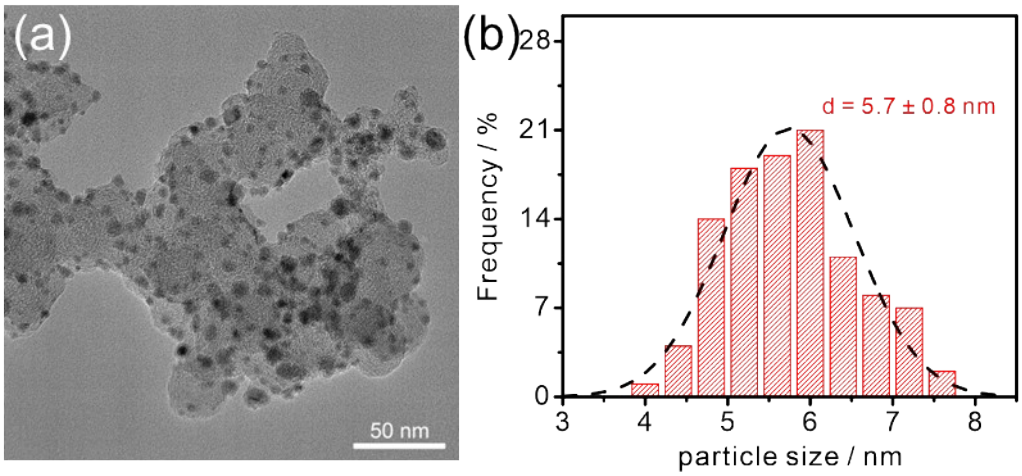

Fig. S4 (a) Low-magnification TEM image of RuGa/C-700 and (b) corresponding histogram of particle size distribution.

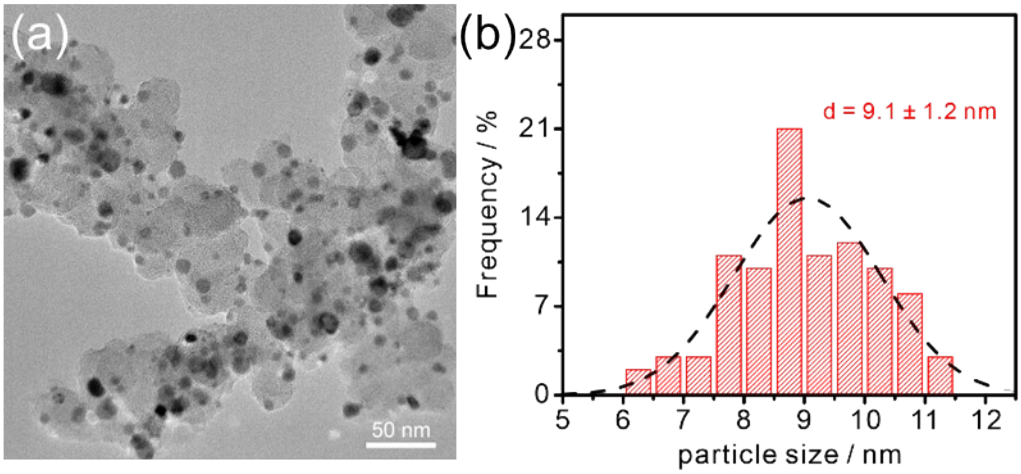

Fig. S5 (a) Low-magnification TEM image of RuGa/C-800 and (b) corresponding histogram of particle size distribution.

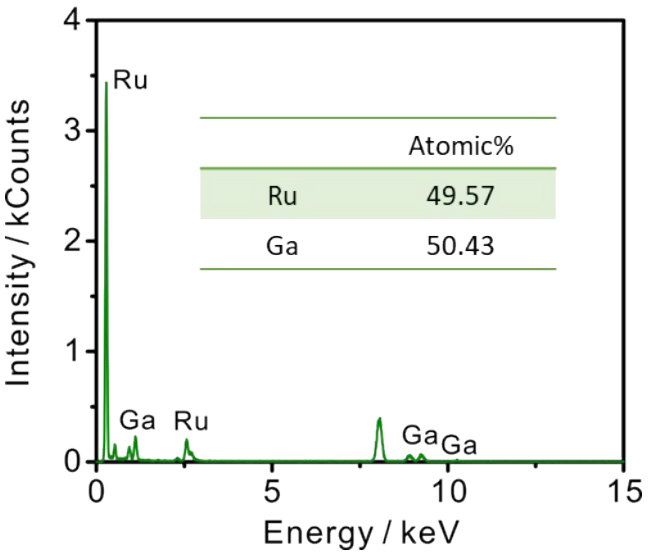

Fig. S6 EDX image of the RuGa/C-600, illustrated by the atomic ratio of Ru and Ga.

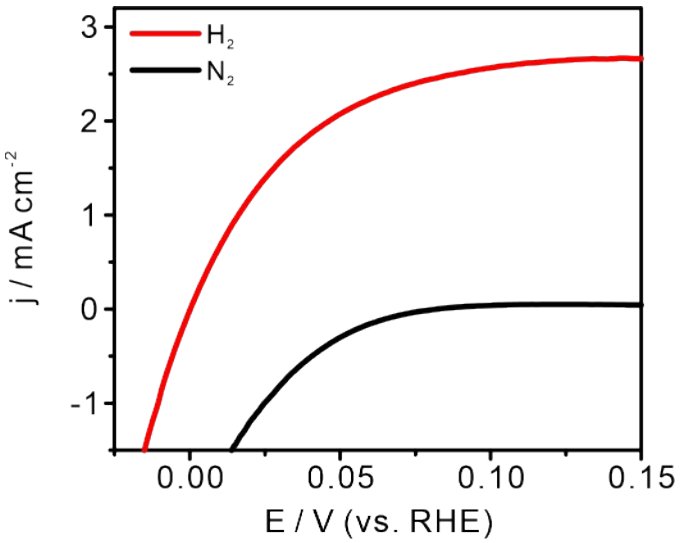

Fig. S7 HOR polarization curves of RuGa/C-600 in H_2 and N_2-saturated 0.1 M KOH electrolytes at the rotation speed of 1,600 rpm.

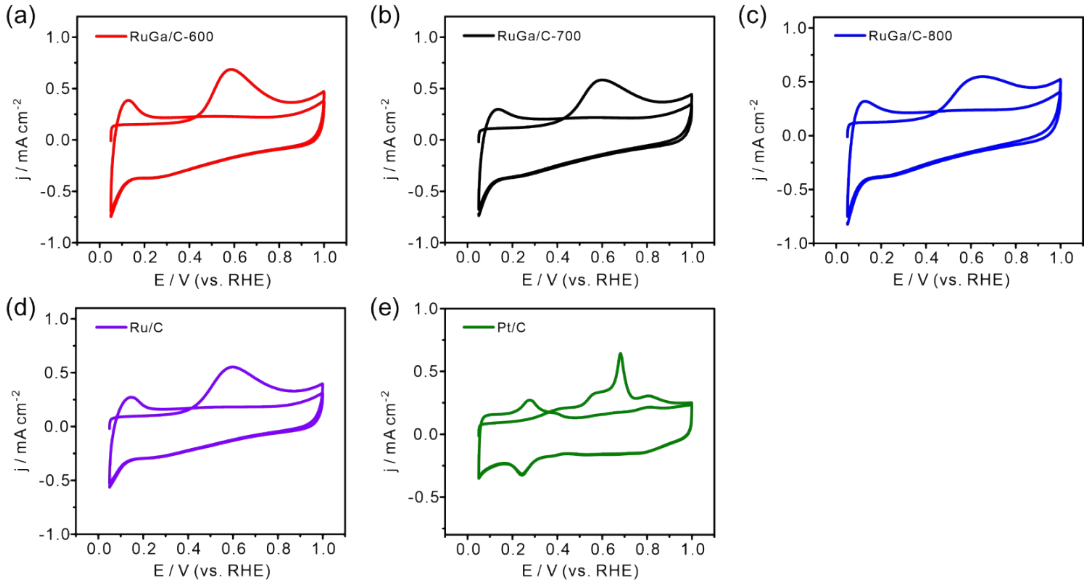

Fig. S8 CO stripping curves of (a) RuGa/C-600, (b) RuGa/C-700, (c) RuGa/C-800, (d) Ru/C, and (e) Pt/C.

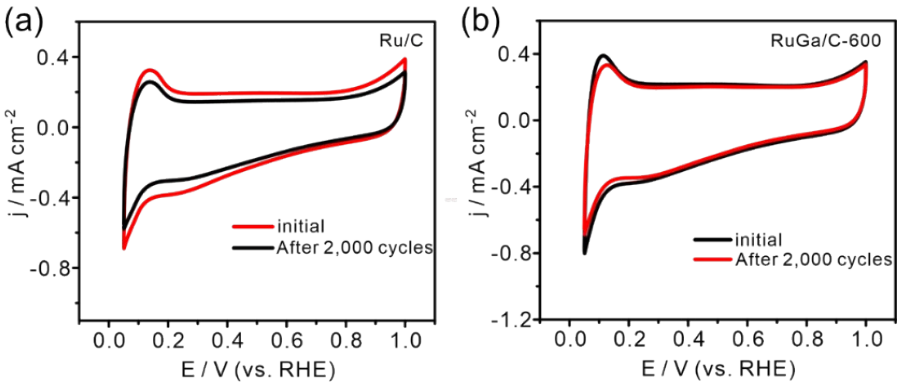

Fig. S9 CV curves of (a) RuGa/C-600 and (b) Ru/C before and after 2,000 cycles.

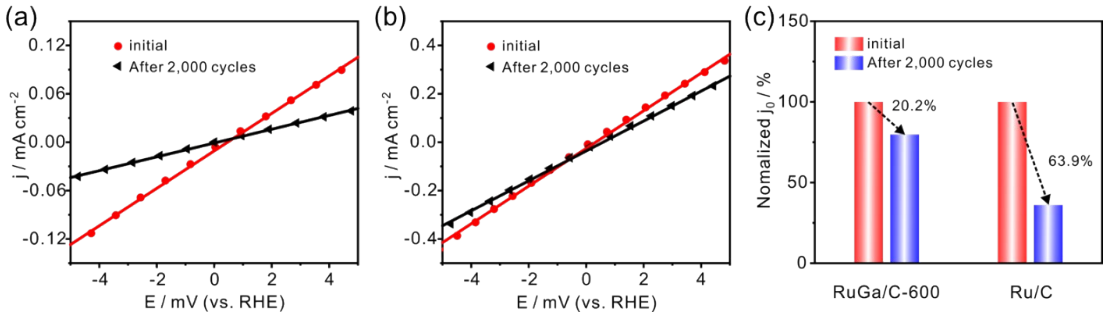

Fig. S10 HOR micro-polarization curves of (a) RuGa/C-600 and (b) Ru/C before and after 2,000 cycles. (c) The exchange current density comparison before and after 2,000 cycles.

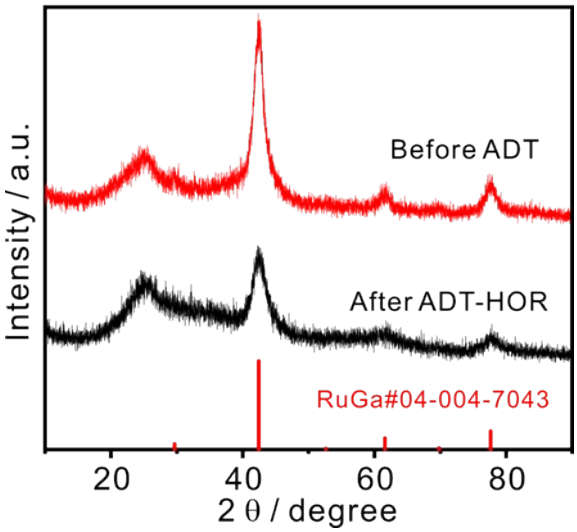

Fig. S11 XRD pattern of RuGa/C-600 after HOR stability.

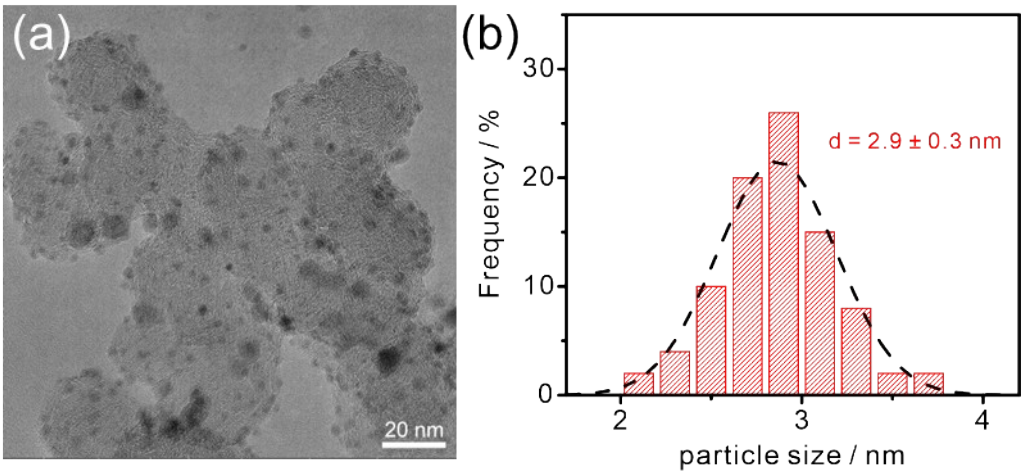

Fig. S12 (a) Low-magnification TEM image of RuGa/C-600 and (b) corresponding histogram of particle size distribution after HOR stability.

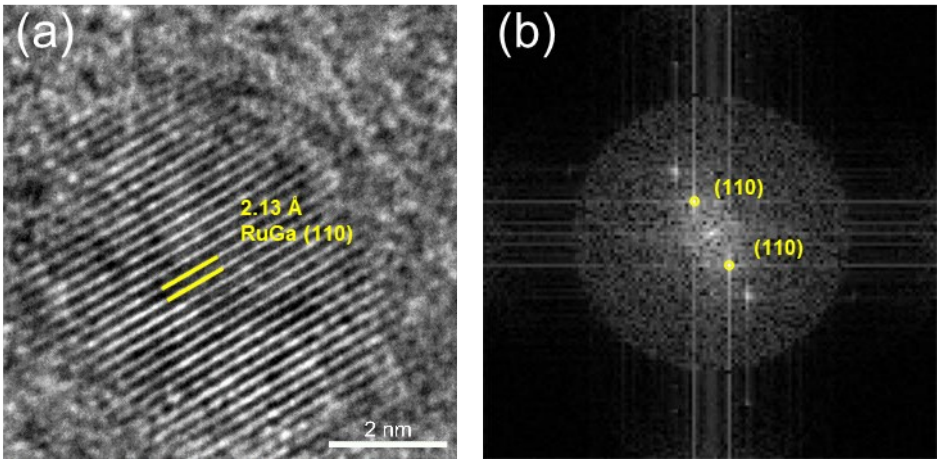

Fig. S13 (a) HRTEM image of RuGa/C-600 and (b) corresponding FFT pattern after HOR stability.

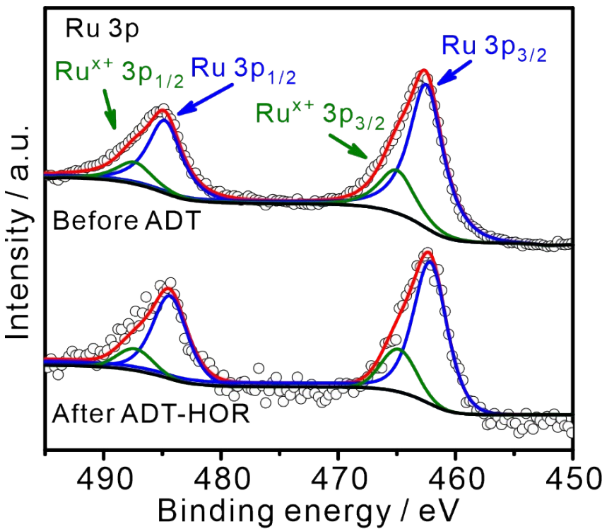

Fig. S14 Ru 3p XPS spectrum of RuGa/C-600 after HOR stability.

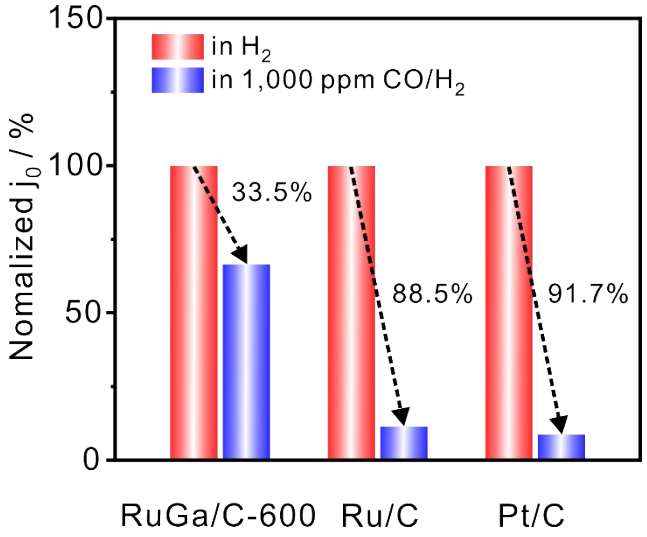

Fig. S15 Loss of exchange current density with 1,000 ppm CO.

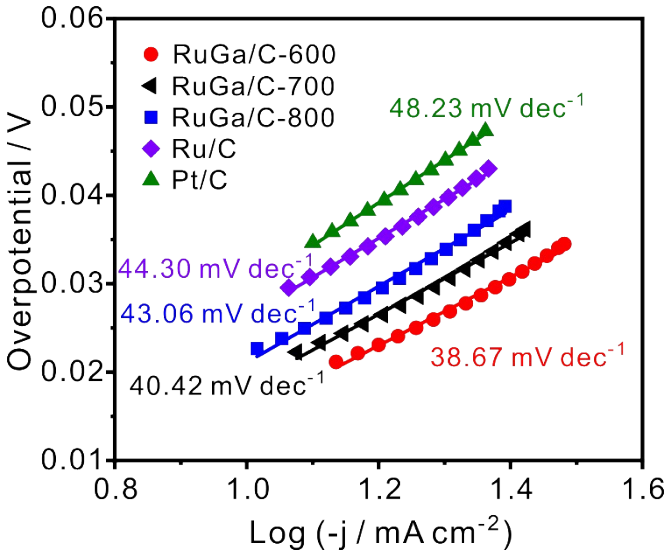

Fig. S16 HER Tafel slopes of RuGa/C, Ru/C, and Pt/C.

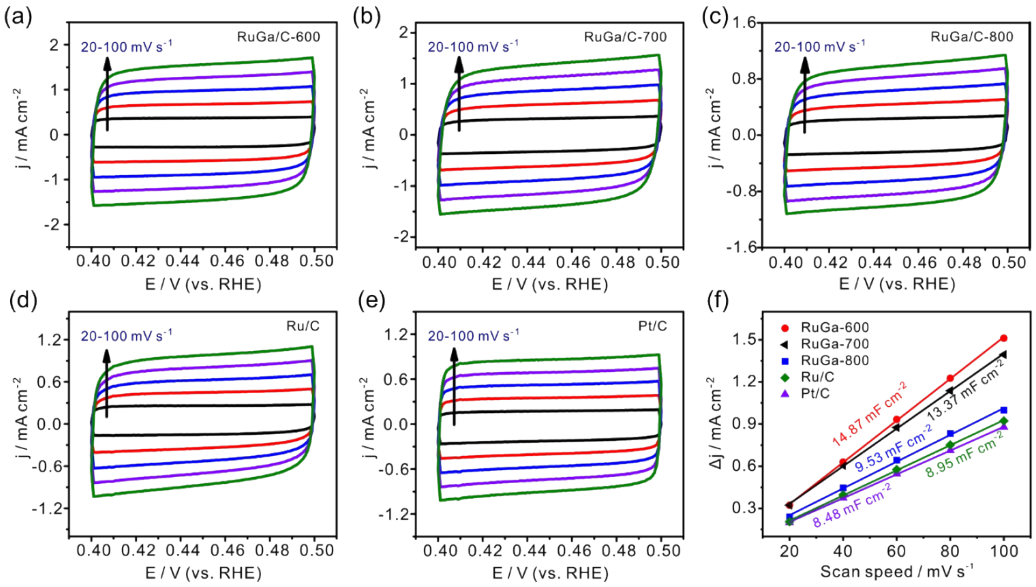

Fig. S17 CV curves recorded at various scan speeds from 20 mV s^{-1} to 100 mV s^{-1} for (a) RuGa/C-600, (b) RuGa/C-700, (c) RuGa/C-800, (d) Ru/C, and (e) Pt/C. (f) Corresponding double-layer capacitances.

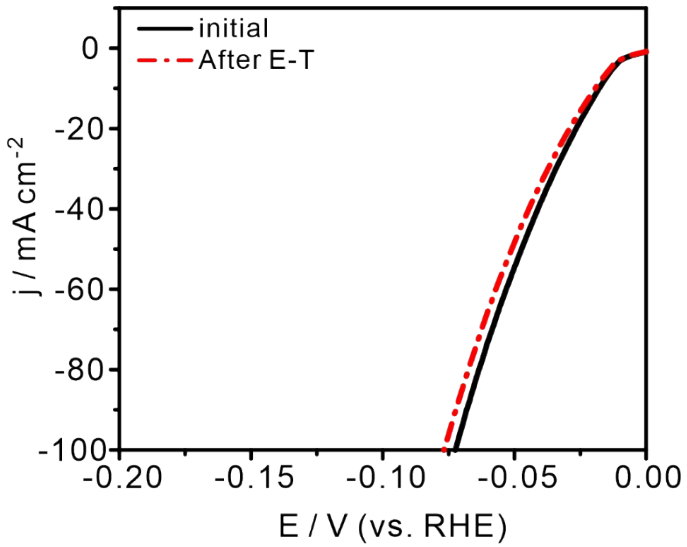

Fig. S18 HER polarization curves before and after the chronopotentiometry test.

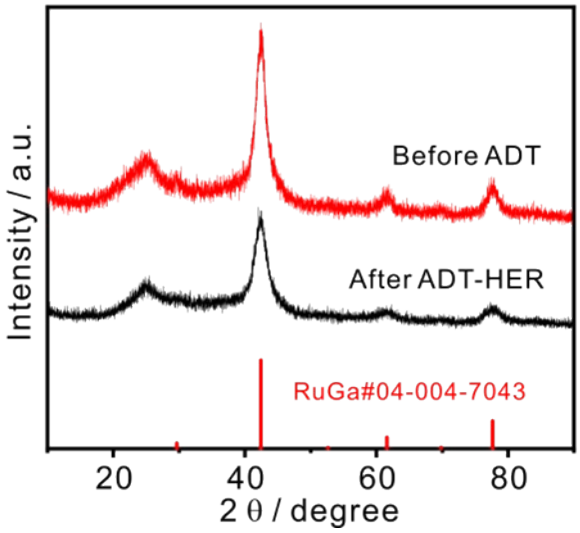

Fig. S19 XRD pattern of RuGa/C-600 after HOR stability.

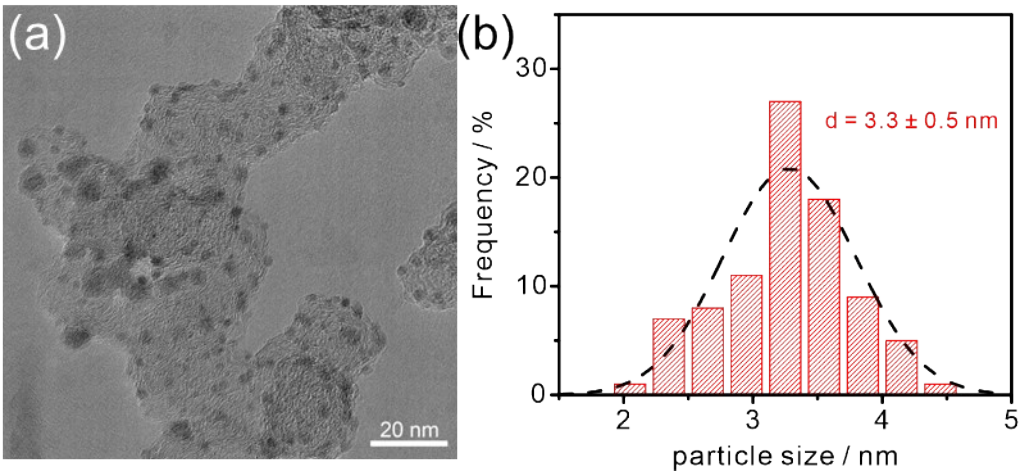

Fig. S20 (a) Low-magnification TEM image of RuGa/C-600 and (b) corresponding histogram of particle size distribution after HER stability.

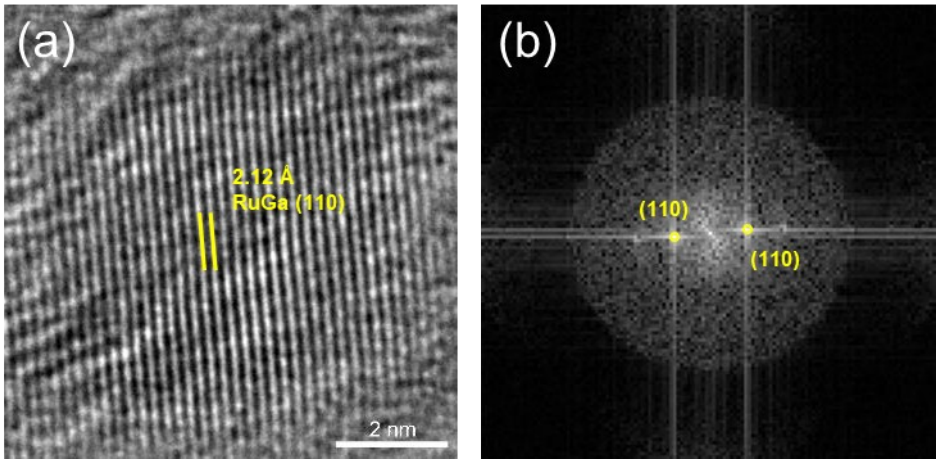

Fig. S21 (a) HRTEM image of RuGa/C-600 and (b) corresponding FFT pattern after HER stability.

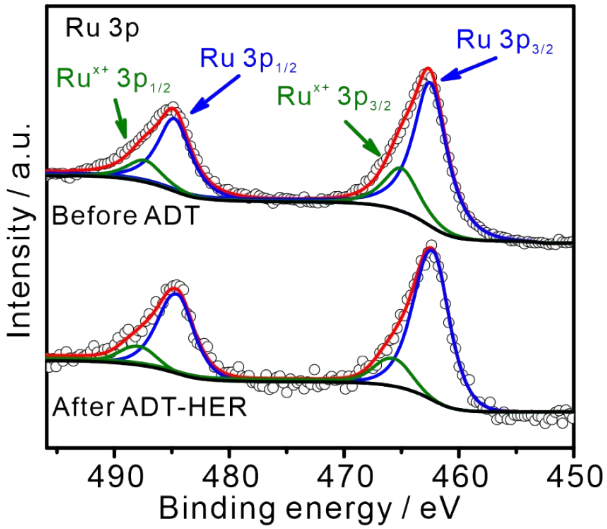

Fig. S22 Ru 3p XPS spectrum of RuGa/C-600 after HER stability.

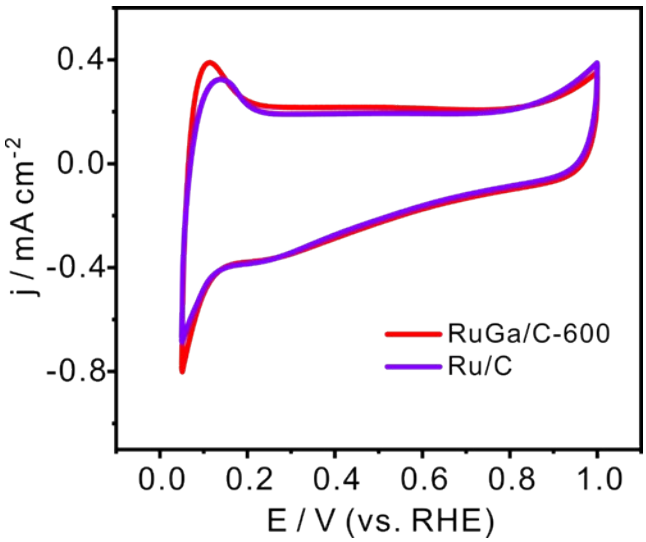

Fig. S23 CV curves of RuGa/C-600 and Ru/C.

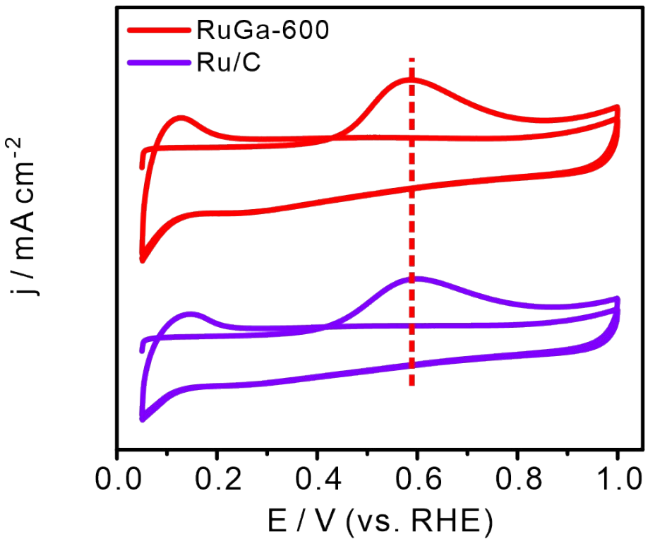

Fig. S24 CO stripping curves of RuGa/C-600 and Ru/C.

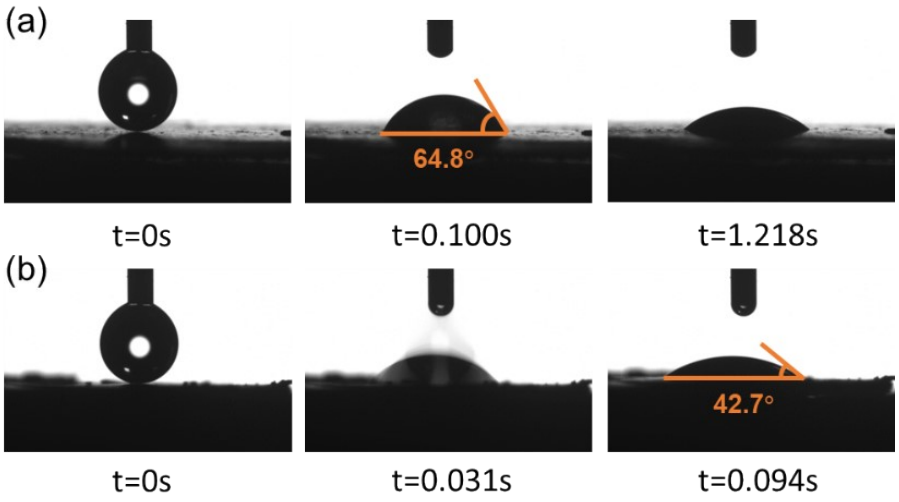

Fig. S25 Water contact angles of (a) Ru/C and (b) RuGa/C-600.

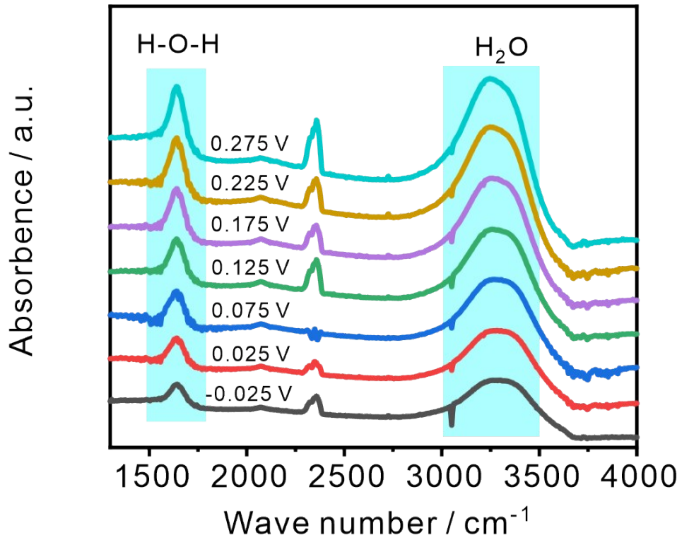

Fig. S26 The in situ ATR-SEIRAS spectra recorded at potentials from -0.025 V to 0.275 V vs RHE for Ru/C.

Supplementary Tables

Table S1 Particle sizes of RuGa/C-600, RuGa/C-700, and RuGa/C-800 calculated by the Debye-Scherrer equation.

Catalysts	Size (nm)
RuGa/C-600	6.02
RuGa/C-700	9.36
RuGa/C-800	12.04

Table S2 LRO degrees of RuGa/C-600, RuGa/C-700, and RuGa/C-800 based on the ratio of super-lattice (100) and fundamental lattice (110).

Catalysts	LRO (%)
RuGa/C-600	73.86
RuGa/C-700	84.85
RuGa/C-800	90.91

Table S3 Summary of binding energies for Ru $3p_{3/2}$ and Ru $3p_{1/2}$ of Ru/C and RuGa/C-600 from XPS results, respectively.

Catalysts	Binding Energy (eV)			
	$Ru^0{}_{3/2}$	$Ru^{4+}{}_{3/2}$	$Ru^0{}_{1/2}$	$Ru^{4+}{}_{1/2}$
Ru/C	462.83	465.11	485.05	487.43
RuGa/C-600	462.48	465.01	484.67	487.38

Table S4 The content of Ru and Ga tested by EDX.

Element	Atomic fraction (%)	Atomic error (%)	Mass fraction (%)	Mass error (%)
Ru	49.57	4.21	58.76	4.08
Ga	50.43	5.21	41.24	4.08

Table S5 The content of Ru and Ga tested by ICP-OES.

Catalysts	Mass ratio		Molar ratio
	Ru (%)	Ga (%)	Ru : Ga (%)
RuGa/C-600	15.86	11.53	48.69 : 51.31
RuGa/C-700	15.87	11.51	48.75 : 51.25
RuGa/C-800	15.77	11.45	48.72 : 51.28
Ru/C	19.94	/	/

Table S6 Summary of the exchange current density calculated from micro-polarization regions and Tafel regions. The transfer coefficient (α) is also listed.

Catalysts	Exchange current density (mA cm^{-2})	
	Micro-polarization regions	**Tafel regions**
RuGa/C-600	2.03	2.08 (a=0.83)
RuGa/C-700	1.17	1.13 (a=0.62)
RuGa/C-800	0.69	0.64 (a=0.52)
Ru/C	0.61	0.52 (a=0.37)
Pt/C	1.38	1.31 (a=0.84)

Table S7 Summary of the ECSAs, exchange current density (j_0), kinetic current density (j_k), specific activity ($j_{0,ECSA}$), and mass activity ($j_{k,m}$) for catalysts in Figure 3e.

Catalysts	ECSA	j_0	$j_{k@50mV}$	$j_{0,ECSA}$ (mA cm_{PGM}^{-2})	$j_{k,m@50mV}$ (mA μg_{PGM}^{-1})
RuGa/C-600	0.78	2.03	8.95	0.54	1.84
RuGa/C-700	0.72	1.17	3.31	0.33	0.68
RuGa/C-800	0.57	0.69	1.57	0.25	0.33
Ru/C	0.54	0.61	0.94	0.19	0.15
Pt/C	0.53	1.38	5.44	0.43	0.89

Table S8 HOR performance of reported catalysts in alkaline electrolytes.

Catalysts	Loading (μg_{PGM} cm^{-2})	$j_{0,ECSA}$ (mA cm_{PGM}^{-2})	$j_{k,m@50mV}$ (mA μg_{PGM}^{-1})	Reference
RuGa/C-600	**4.86**	**0.54**	**1.84**	**This work**
Ru@C-340	10	0.39	1.2	2
fcc-RuW	12.2	0.67	0.882	4
RuS_2	4.31	0.676	1.437	5
IO-Ru-TiO_2/C	25.48	0.10885	0.907	6
Ni1Ru1/C	12.5	0.078	0.224	7
Ru-TiO/TiO_2@NC	25.5	0.271	0.1702	8
Ru-V_2O_3/OC	22.5	0.10	1.02	9
$RuFe_{0.1}$/C	1.25	0.544	0.934	10
Ga-Ru/C	7.04	0.30	0.593	11
B-Ru/C	7.49	0.316	1.716	12
Ru-Ru_2P/C	8.33	/	1.265	13
hcp/fcc-Ru	6.57	0.664	1.016	14
di-RuNi MLNS/C	3	/	1.79	15
Ru_2P/C	9.26	/	0.558	13
Ru/NC@WOC	32.1	/	1.96	16

Table S9 HER performance of reported catalysts in alkaline electrolytes.

Catalysts	Electrolyte	Loading (mg_{cat} cm^{-2})	Overpotential (mV@10 mA cm^{-2})	Tafel slope (mV dec^{-1})	Reference
RuGa/C-600	**1 M KOH**	**0.255**	**18**	**38.67**	**This work**
RuAu-0.2	1 M KOH	/	24	27	17
Pd@Ru NRs	1 M KOH	/	30	30	18
P-Ru/C	1 M KOH	0.03	31	105	19
Ru/WC_x	1 M KOH	0.8	29	43	20
Ru-N(O)-C	1 M KOH	0.	39	49	21
Ru@CDs	1 M KOH	/	30	22	22
NiRu@Fe/C@CNT	1 M KOH	/	32	54	23
V_O-Ru/HfO_2-OP	1 M KOH	/	39	29	24
c/a-Ru/VO_x-500	1 M KOH	0.425	33	27	25
Ru_1CoP/CDs	1 M KOH	0.42	51	73.4	26
Ru-NPs/SAs@N-TC	1 M KOH	0.282	97	58	27
Ru/TiN-300	1 M KOH	/	38	39	28
$Ru/MoSe_2$@MHCS	1 M KOH	0.40	38.4	30.24	29
RuCo	1 M KOH	/	24.9	40.5	30
Ru-MoS_2/CNT	1 M KOH	/	50	62	31

Table S10 FWHM, proportion, and peak potential of deconvoluted peak H1 and H2 for RuGa/C-600 and Ru/C

	H1 (V)	**FWHM**	**Proportion (%)**	**H2 (V)**	**FWHM**	**Proportion (%)**
RuGa/C-600	0.108	0.054	60.27	0.149	0.063	39.73
Ru/C	0.123	0.056	49.11	0.163	0.059	50.89

References

1. Y. Xiong, Y. Yang, H. Joress, E. Padgett, U. Gupta, V. Yarlagadda, D. N. Agyeman-Budu, X. Huang, T. E. Moylan, R. Zeng, A. Kongkanand, F. A. Escobedo, J. D. Brock, F. J. DiSalvo, D. A. Muller and H. D. Abruña, *Proc. Natl. Acad. Sci. U. S. A.*, 2019, **116**, 1974-1983.
2. Z. Yang, W. Lai, B. He, J. Wang, F. Yu, Q. Liu, M. Liu, S. Zhang, W. Ding, Z. Lin and H. Huang, *Adv. Energy Mater.*, 2023, **13**, 2300881.
3. L. Wang, Z. Xu, C. H. Kuo, J. Peng, F. Hu, L. Li, H. Y. Chen, J. Wang and S. Peng, *Angew. Chem., Int. Ed.*, 2023, **62**, e202311937.
4. Y. Li, J. Yue, C. Yang, H. Jia, H. Cong and W. Luo, *J. Energy Chem.*, 2024, **92**, 207-215.
5. C. Yang, J. Yue, G. Wang and W. Luo, *Angew. Chem., Int. Ed.*, 2024, **63**, e202401453.
6. J. Jiang, S. Tao, Q. He, J. Wang, Y. Zhou, Z. Xie, W. Ding and Z. Wei, *J. Mater. Chem. A*, 2020, **8**, 10168-10174.
7. J. Liu, J. Wang, Y. Fo, B. Zhang, C. Molochas, J. Gao, W. Li, X. Cui, X. Zhou, L. Jiang and P. Tsiakaras, *Chem. Eng. J.*, 2023, **454**, 139959.
8. L. Jing, G. Jie, W. Yu, H. Ren, X. Cui, X. Chen and L. Jiang, *Chem. Eng. J.*, 2023, **472**, 145009.
9. P. Wang, Y. Yang, W. Zheng, Z. Cheng, C. Wang, S. Chen, D. Wang, J. Yang, H. Shi, P. Meng, P. Wang, H. Tong, J. Chen and Q. Chen, *J. Am. Chem. Soc.*, 2023, **145**, 27867-27876.
10. Y. Li, C. Yang, C. Ge, N. Yao, J. Yin, W. Jiang, H. Cong, G. Cheng, W. Luo and L. Zhuang, *Small*, 2022, **18**, 2202404.
11. L. Wu, L. Su, Q. Liang, W. Zhang, Y. Men and W. Luo, *ACS Catal.*, 2023, **13**, 4127-4133.
12. P. Han, X. Yang, L. Wu, H. Jia, J. Chen, W. Shi, G. Cheng and W. Luo, *Adv. Mater.*, 2023, **36**, 2304496.
13. L. Su, Y. Jin, D. Gong, X. Ge, W. Zhang, X. Fan and W. Luo, *Angew. Chem., Int. Ed.*, 2023, **62**, e202215585.
14. Y. Li, C. Yang, J. Yue, H. Cong and W. Luo, *Adv. Funct. Mater.*, 2023, **33**, 2211586.
15. Y. Dong, Q. Sun, C. Zhan, J. Zhang, H. Yang, T. Cheng, Y. Xu, Z. Hu, C. W. Pao, H. Geng and X. Huang, *Adv. Funct. Mater.*, 2022, **33**, 2210328.
16. Y. Yang, X. Shao, S. Zhou, P. Yan, T. T. Isimjan and X. Yang, *ChemSusChem*, 2021, **14**, 2992-3000.
17. C. H. Chen, D. Wu, Z. Li, R. Zhang, C. G. Kuai, X. R. Zhao, C. K. Dong, S. Z. Qiao, H. Liu and X. W. Du, *Adv. Energy Mater.*, 2019, **9**, 1803913.
18. Y. Luo, X. Luo, G. Wu, Z. Li, G. Wang, B. Jiang, Y. Hu, T. Chao, H. Ju, J. Zhu, Z. Zhuang, Y. Wu, X. Hong and Y. Li, *ACS Appl. Mater. Interfaces*, 2018, **10**, 34147-34152.
19. Y. Zhao, X. Wang, G. Cheng and W. Luo, *ACS Catal.*, 2020, **10**, 11751-11757.
20. X. Chen, C. Chen, M. M. Amjad, D. Sun, B. Sun and K. Zhang, *Appl. Catal., B*, 2024, **344**, 123644.
21. M. Lao, G. Zhao, P. Li, T. Ma, Y. Jiang, H. Pan, S. X. Dou and W. Sun, *Adv. Funct. Mater.*, 2021, **31**, 2100698.
22. Z. Liu, B. Li, Y. Feng, D. Jia, C. Li, Q. Sun and Y. Zhou, *Small*, 2021, **17**, e2102496.

23. T. Gao, X. Li, X. Chen, C. Zhou, Q. Yue, H. Yuan and D. Xiao, *Chem. Eng. J.*, 2021, **424**, 130416.
24. G. Li, H. Jang, S. Liu, Z. Li, M. G. Kim, Q. Qin, X. Liu and J. Cho, *Nat. Commun.*, 2022, **13**, 1270.
25. Z. Tao, H. Zhao, N. Lv, X. Luo, J. Yu, X. Tan and S. Mu, *Adv. Funct. Mater.*, 2024, **34**, 2312987.
26. H. Song, M. Wu, Z. Tang, J. S. Tse, B. Yang and S. Lu, *Angew. Chem., Int. Ed.*, 2021, **60**, 7234-7244.
27. B. Yan, D. Liu, X. Feng, M. Shao and Y. Zhang, *Adv. Funct. Mater.*, 2020, **30**, 2003007.
28. X. Wang, X. Yang, G. Pei, J. Yang, J. Liu, F. Zhao, F. Jin, W. Jiang, H. Ben and L. Zhang, *Carbon Ener.*, 2023, **6**, e391.
29. Y. Kuang, W. Qiao, F. Yang and L. Feng, *J. Energy Chem.*, 2023, **85**, 447-454.
30. V. Jose, V. H. Do, P. Prabhu, C. K. Peng, S. Y. Chen, Y. Zhou, Y. G. Lin and J. M. Lee, *Adv. Energy Mater.*, 2023, **13**, 2301119.
31. X. Zhang, F. Zhou, S. Zhang, Y. Liang and R. Wang, *Adv. Sci.*, 2019, **6**, 1900090.